Earth and Planetary Science Letters 409 (2015) 23–31

Contents lists available at ScienceDirect

Earth and Planetary Science Letters

www.elsevier.com/locate/epsl

High silica granites: Terminal porosity and crystal settling in shallow magma chambers

Cin-Ty A. Lee [a,*], Douglas M. Morton [b]

[a] Department of Earth Science, MS-126, Rice University, Houston, TX, United States
[b] Department of Earth Sciences, United States Geological Survey, University of California, Riverside, United States

ARTICLE INFO

Article history:
Received 7 August 2014
Received in revised form 1 October 2014
Accepted 6 October 2014
Available online xxxx
Editor: An Yin

Keywords:
granite
pluton
cumulate
settling
high silica granite
rhyolite

ABSTRACT

High silica (>70 wt.% SiO_2) granites (HSGs) are important carriers of highly incompatible elements, thus, understanding their origin is relevant to understanding how the composition of the continental crust evolves. We examined a large-scale geochemical study of plutons in the Peninsular Ranges Batholith in southern California (USA) to better understand the petrogenetic relationships between HSGs and the batholith. Using highly incompatible and compatible elements, we show that HSGs represent residual liquids within a felsic (69–72 wt.% SiO_2) magmatic crystal mush at crystal fractions of 50–60% and residual liquid fractions of 40–50%. Trace element systematics show that separation of the HSG liquid from the crystal mush is inefficient, such that no more than 70–80% of the HSG is fully extracted and the remaining greater than 20–30% remains trapped in cumulate mush. We find little evidence of more efficient liquid–crystal segregation, which suggests that compaction-induced segregation may be too slow to be important on a large scale. Instead, the terminal porosity of 20–30% coincides with theoretical maximum packing fraction of unimodal particles settled out of suspension (~0.74), which may indicate that crystal settling – perhaps in the form of hindered settling – drives segregation of viscous silicic melts and crystals. Unlike compaction, settling operates on timescales of 1–10 ky, fast enough to generate large volumes of HSG and complementary cumulates with trapped melt before magma chambers freeze. Many felsic plutons may thus be cumulates, but because of trapped melt, they are difficult to geochemically distinguish from plutons whose compositions fall along liquid lines of descent. The approach here, using a combination of highly incompatible and compatible elements, provides a way of identifying and quantifying trapped melt fractions. Finally, we show that HSGs appear to form only in the shallow crust (<10 km) and rarely in the middle to lower crust. Where HSGs are common, mafic magmas are common too, suggesting a genetic relationship between the two. If HSGs derive by crystal fractionation of basaltic parents, they represent at most 5% of the original mass of parental magma, but because they form almost exclusively at low pressures, they may be over-represented in shallowly exhumed batholiths. Why HSGs form primarily in the upper crust is unclear.

1. Introduction

The tops of many felsic magma bodies contain large volumes of high silica (>70 wt.% SiO_2) granites (HSGs) (Bachl et al., 2001; Bachmann and Bergantz, 2004, 2008; Hildreth, 1979; Hildreth and Wilson, 2007). Understanding how HSGs form is important: many ore deposits associate with HSGs; highly incompatible elements, like K, are transported by HSGs; and large, catastrophic rhyolite eruptions may be related to HSGs (Bachmann and Bergantz, 2004, 2008). There is a general agreement that most HSGs form by crystal–liquid segregation from a cooling and crystallizing magma, but how segregation occurs is unknown. Do HSGs represent the residual melt formed by crystal settling or by expulsion from a compacting magmatic mush (crystals+melt)? Forming large volumes of HSG must be accompanied by a complementary reservoir of cumulates (Gelman et al., 2014). Segregation must be complete before magmas freeze, but compaction timescales are poorly constrained and magma chamber lifespans are debated. One way to constrain the dominant segregation process is to study the hypothetical cumulates, but where are these lithologies? Felsic plutons have been suggested to be the "missing" cumulates (Gelman et al., 2014; Mills et al., 2012), but their compositions can also be modeled as frozen liquids. Here, we show that the complementary cumulates are indeed disguised among the felsic plutons, not as pure crystal cumulate, but as frozen mixtures of crystals and

* Corresponding author.
E-mail address: ctlee@rice.edu (C.-T.A. Lee).

http://dx.doi.org/10.1016/j.epsl.2014.10.040
0012-821X/

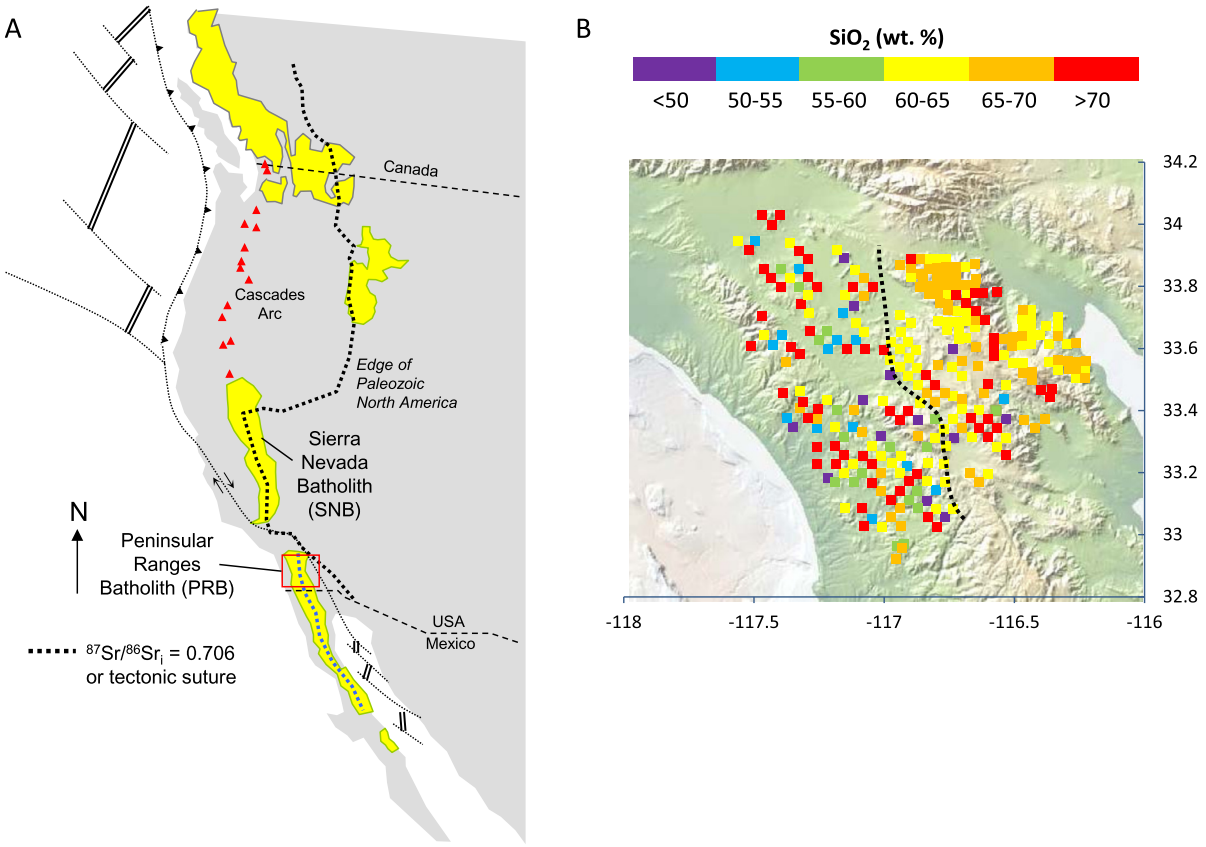

Fig. 1. A. Map of North America showing location of Cretaceous to early Paleocene continental arcs in yellow. Northern Peninsular Ranges Batholith (PRB) shown as inset. Dotted black line represents initial $^{87}Sr/^{86}Sr$ contour (Kistler and Peterman, 1973). Other lines denote plate boundaries. B. Elevation map of southern California with locations of PRB sampling, color-coded for SiO_2 content in weight% on a volatile-free basis. Data are from (Lee et al., 2007). Dashed line represents the boundary between western and eastern PRB, the former emplaced through thin Jurassic island arc-accreted crust and the latter through Paleozoic or older North American basement (Lee et al., 2007; Morton et al., 2014). (For interpretation of the references to color in this figure legend, the reader is referred to the web version of this article.)

trapped HSG melt, making them geochemically similar to liquids. What is new here is that we provide a means of quantifying the fraction of this trapped melt.

2. Regional database: the Peninsular Ranges Batholith

To explore crystal–liquid segregation scenarios on a batholith scale, we examined a regional database of plutonic rocks in the Peninsular Ranges Batholith (PRB) in southern California (Lee et al., 2007) (Fig. 1). The PRB consists of plutonic rocks (mostly tonalites and granodiorites) formed in a Cretaceous continental arc associated with the subduction of the Farallon plate beneath North America. The plutonic rocks have compositions typical of calc-alkaline (Fe-depleting) differentiation trends seen in many continental arcs. The database consists of rocks sampled along systematic grid points, and at each grid point, samples of equivalent weight from the corners of a 400 × 400 foot square grid were crushed and homogenized to generate a space-averaged sample (Baird et al., 1979). This approach was done to avoid sampling bias associated with small-scale heterogeneities. To minimize the effects of crustal assimilation or re-melting of pre-existing crust, we focus primarily on the western PRB (Fig. 1), which based on unradiogenic strontium isotopes, appears to have interacted less with the crustal basement than plutons in the east (Kistler et al., 2003; Lee et al., 2007; Morton et al., 2014). All data used in this paper have already been published in (Lee et al., 2007), but interpretations presented here are new.

3. Cumulate identification using highly compatible and highly incompatible elements

Because we are interested in identifying cumulates, we focus on highly compatible and incompatible elements, the former strongly partitioned into crystallizing phases and depleted in the liquid, and the latter strongly partitioned into liquids but depleted in crystals. Moderately compatible/incompatible elements do not fractionate enough between solids and liquids and are thus less ideal for distinguishing cumulates and melts. Fig. 2a–d shows variation diagrams of K, Rb, Sr and Eu versus SiO_2. K and Rb (as well as other incompatible elements like Th and U) increase by 25–30 times as SiO_2 increases from gabbro ($SiO_2 \sim 50$ wt.%) to the HSGs ($SiO_2 > 70$ wt.%), indicating that these elements are almost perfectly incompatible, consistent with the dominant minerals in PRB plutons being quartz, plagioclase, and hornblende, none of which accommodate significant amounts of Rb and K. The extreme enrichments in Rb and K, even in the HSGs, is also consistent with the suggestion that K-feldspar is a late crystallizing phase in typical I-type granitoids and does not participate in crystal–melt segregation (Glazner and Johnson, 2013). In contrast, Sr decreases and Eu remains relatively constant with increasing SiO_2, with both elements plummeting after SiO_2 increases beyond 71 wt.%. Such behavior reflects the strong compatibility of Sr and the moderate compatibility of Eu in plagioclase. We note that the inferred geochemical behaviors of K and Rb can be generalized for typical I-type granitoids, but not for alkalic granites in which biotite or alkali feldspar may be early crystallizing phases (Bucholz et al., 2014).

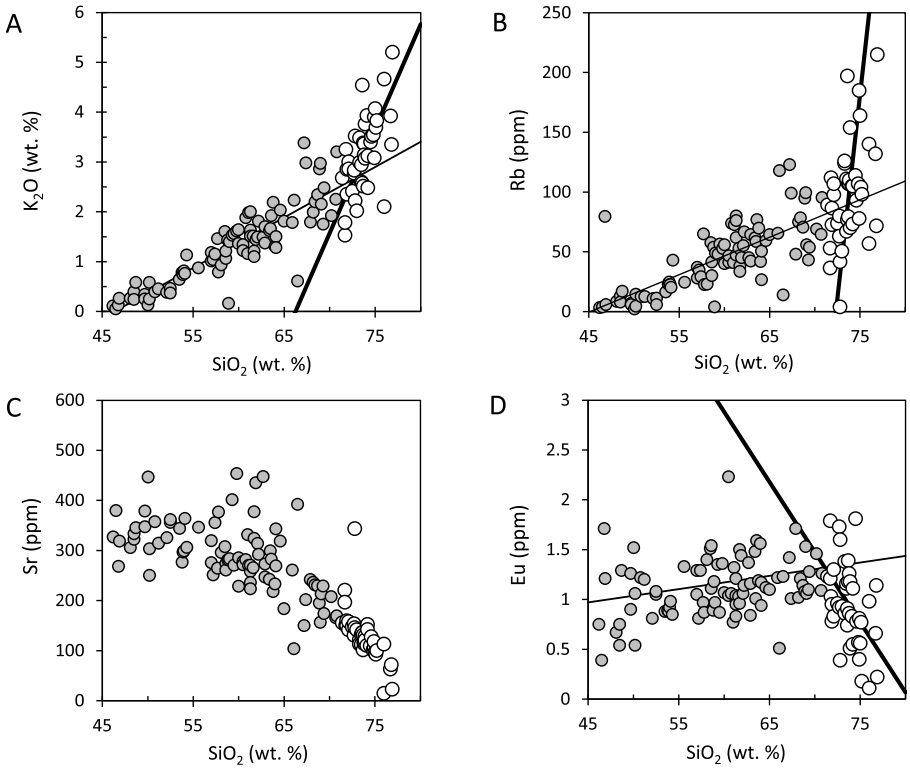

Fig. 2. A–D show K_2O (wt.%), Rb (ppm), Sr (ppm) and Eu (ppm) versus SiO_2 (wt.%) for PRB rocks in Fig. 1. Samples with <71 wt.% SiO_2 are gray and >71 wt.% SiO_2 are open. K_2O and Rb increase with increasing SiO_2 indicating they are highly incompatible. Sr is compatible. Eu is moderately incompatible, but becomes highly compatible after 71 wt.% SiO_2. Lines represent total (orthogonal) linear regression through samples < 71 wt.% SiO_2 and >71 wt.% SiO_2. All concentrations are on a volatile-free basis.

Of particular interest is that the slopes of these variation diagrams change abruptly at ~71 wt.% SiO_2 due to marked enrichment of incompatible element concentrations and a marked depletion in compatible elements with further increase in SiO_2 (Figs. 2a–d). This change in behavior at ~71 wt.% SiO_2, however, is unlikely to be due to a sudden change in element compatibility alone. For example, to cause such a decrease in Sr and Eu requires a two-fold increase in compatibility but the change in plagioclase crystallizing mode and the change in melt composition is too small to yield such a large change in compatibility. It is particularly difficult to explain the rise in K and Rb by any further decrease in compatibility because these elements, already highly incompatible, cannot behave any more incompatibly. Instead, the apparent decrease in compatibility of Rb and K and increase in compatibility of Sr and Eu is an artifact of the rate at which melt SiO_2 increases with decreasing melt fraction at SiO_2 contents above ~70 wt.%. This effect can be seen in Fig. 3a, where we plot SiO_2 versus melt fraction F_b relative to the basaltic parent, where F_b is estimated from the inverse of the enrichment factor of an incompatible element ($C/C_{o(basalt)} \sim 1/F_b$ for a perfectly incompatible element, where $C_{o(basalt)}$ is the trace element composition of the basaltic parent). To estimate $C_{o(basalt)}$ for Rb and K, we linearly regressed Rb- and K_2O–SiO_2 data for those samples with $SiO_2 < 71$ wt.% and then took the extrapolated Rb and K_2O concentrations at 50 wt.% SiO_2 as $C_{o(basalt)}$. If HSGs derive by fractionation from a basaltic parent (Jagoutz and Schmidt, 2012; Lee and Bachmann, 2014; Putirka et al., 2014), Fig. 3a shows that they represent the last <5% of liquids remaining after crystallization of a basaltic parent.

Regardless of whether the granites derive from basaltic parents, what is clear is that the HSGs themselves derive from an already silicic parental melt (~69–72 wt.% SiO_2), corresponding to the position of the kink in the variation diagrams in Fig. 2. Mass balance requires that the cumulate complement plots along a vector pointing in the opposite direction of that defined by the HSG array, which we define here by linear regression of data with >71 wt.% SiO_2. It follows that the SiO_2 content of the crystal cumulate must be equal to or lower than that of the silicic parent. For compatible elements, like Sr and Eu, no unique cumulate composition can be inferred (Fig. 3), but highly incompatible elements like K, Rb and Th should be nearly zero in crystal cumulates, so the x-intercepts of Th– (not shown), Rb– and K–SiO_2 diagrams bound the minimum SiO_2 content of the crystal cumulate to be between 66 and 72 wt.% (Fig. 2a, b and Fig. 3b). While there are numerous plutons with such high silica contents, there are almost no samples that also have the predicted extreme depletions in K and Rb. Sampling bias is unlikely given our systematic uniform sampling approach of an entire batholith (Fig. 1b). It is also unlikely that these silicic crystal cumulates are hidden in the deep crust because exposed arc sections and seismic velocity models indicate that the lower crust is generally mafic (Ducea and Saleeby, 1998; Greene et al., 2006; Jagoutz and Schmidt, 2012; Lee, 2014; Lee et al., 2006).

4. Trapped melt in cumulate

One way to reconcile the apparent lack of geochemical evidence for crystal cumulates in the crust is if a significant fraction of HSG melt is trapped, such that the bulk cumulate (crystals + trapped melt) has higher incompatible and lower compatible element concentrations, making the cumulate look geochemically more like a liquid than a pure solid upon freezing (Langmuir, 1989). Such cumulates would be expected to fall somewhere between the crystal cumulate (no trapped melt) and the silicic parent on element–element diagrams. Candidates for cumulates containing trapped melt are clearly evident in Fig. 2. Calculating the amount of trapped melt is straightforward. Assuming equilibrium

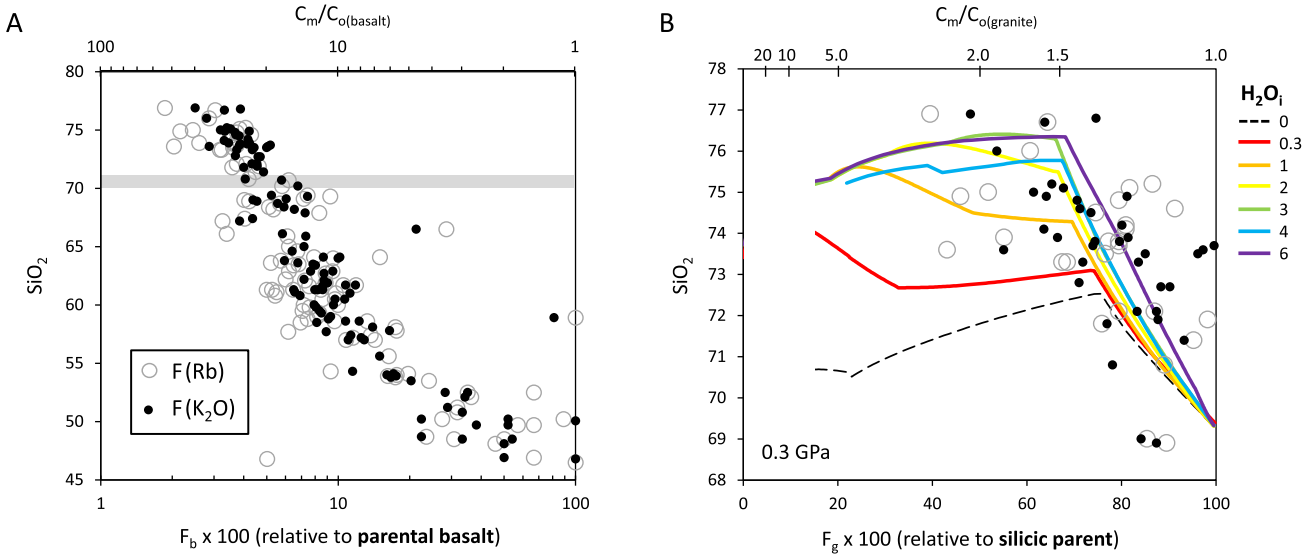

Fig. 3. A. SiO_2 (wt.% on volatile-free basis) versus melt fraction F_b (×100) relative to a parental basalt/gabbro composition from the PRB. F_b is estimated by the inverse of the enrichment factor of an incompatible element, such as Rb (open circle) and K (black circle). For samples with $SiO_2 > 71$ wt.%, samples with Rb and K contents less than the silicic parent are not plotted because those samples are cumulates. Gray horizontal bar represents reference line for 71 wt.% SiO_2. B.+ Same as in A but F_g represents melt fraction relative to parental silicic parent of 70–71 wt.%. F_g determined as inverse of Rb and K enrichments in high silica granites relative to a 70–71 wt.% parental magma. Curves in B represent Rhyolite Melts (Gualda et al., 2012) thermodynamic models of the SiO_2 content (on a volatile-free basis) of residual melts during crystallization of 69 wt.% SiO_2 silicic parent for different bulk H_2O contents (f_{O_2} at the fayalite–magnetite-buffer). Calculations were done at 0.3 GPa, which corresponds to the average pressures of equilibration of western PRB plutons. Symbols as in A. In both A and B, top horizontal axis represents inverse enrichment factor of Rb or K in melt relative to that in basalt (A) and silicic parental granite (B).

and mass balance, the composition of the melt C_m relative to that of the silicic bulk system (melt + crystals) C_o is related by the well-known batch melting/crystallization equation,

$$C_m/C_o = 1/\left[F_g + D(1-F_g)\right] \quad (1)$$

where F_g represents the mass fraction of melt in the system (relative to the silicic or granitic parent, e.g., the composition defined by the kink in a K_2O versus SiO_2 plot) and D is the partition coefficient, which is equal to C_x/C_m, where C_x is the concentration of the element of interest in the solid crystals. Here, we assume that the bulk system is the silicic parental melt (not the basaltic parent) since we are now interested in the origin of the HSGs. As the silicic parental magma crystallizes, it undergoes settling or compaction, generating a lower cumulate layer containing crystals ± trapped melt and an upper layer consisting of only melt (Fig. 4d). The composition of the melt in the upper layer is assumed to be the same as that trapped in the cumulate. We then define $f_{me} = M_{me}/M_m$ as the fraction of the melt extracted into the upper layer (where M_{me} is the mass of melt extracted) relative to the total melt remaining in the system M_m (where M_m is the sum of the extracted and trapped melt masses). The composition of the cumulate layer (crystals ± trapped melt) C_{cum} is then

$$C_{cum}/C_o = \left[1 - \frac{f_{me}F_g}{F_g + D(1-F_g)}\right]/(1 - f_{me}F_g) \quad (2)$$

The composition of the melt is given by Eq. (1) and the composition of the crystals is given by $C_x = DC_m$, which is zero for a highly incompatible element. The fraction of trapped melt in the cumulate, that is, the mass of trapped melt divided by the bulk cumulate (trapped melt + crystals), is then given by

$$f_{trap} = \frac{F_g(1-f_{me})}{1-f_{me}F_g} \quad (3)$$

A density correction is needed to convert mass fraction to volume fraction or porosity ϕ of trapped melt, that is, $\varphi = \rho_x f_{trap}/[\rho_m + f_{trap}(\rho_x - \rho_m)]$, where ρ_x is the density of the crystals (2700–2900 kg/m^3) and ρ_m is the density of the melt (2300–2700 kg/m^3), but this relative correction is small compared to the natural variations in HSG composition, which we use to estimate trapped melt fraction.

The geochemistry of the HSGs allows us to constrain F_g, f_{me} and f_{trap}. Taking C_o to represent the Rb or K content of the silicic parent defined by the kink at ~69–72 wt.% SiO_2 (Figs. 2 and 4c), we estimate that the most silicic HSGs define terminal residual melt fractions F_g of 0.4–0.5 relative to the silicic parent (we do not do the mass balance with SiO_2 because of the larger relative errors on the SiO_2 content of the parental silicic magma compared to Rb and K). We can compare these mass balance constraints on F_g with forward models of crystallization using the thermodynamics based program Rhyolite Melts (Gualda et al., 2012). We adopt a starting composition corresponding to tonalites having ~69 wt.% SiO_2 on a volatile-free basis ($Al_2O_3 = 16.04$, $CaO = 4.05$, $Fe_2O_{3T} = 3.64$, $K_2O = 1.49$, $MgO = 1.15$, $Na_2O = 4.13$, $SiO_2 = 69.1$, $TiO_2 = 0.41$ wt.%) and model closed system equilibrium crystallization of this melt for a range of water contents (Lee et al., submitted for publication). We assume 3 kbar pressure, corresponding to the pressures of equilibration in the western PRB as determined by Al-in-hornblende barometry (Ague and Brimhall, 1988). Considering only granitoids with $SiO_2 > 71$ wt.%, it can be seen that the observed SiO_2–F_g array overlaps that predicted by thermodynamic modeling for bulk H_2O greater than 2 wt.% (Fig. 3b).

We can also compare modeled temperature–F_g or temperature–SiO_2 relationships to calculated temperatures based on the bulk Zr contents of the plutons assuming plutons with $SiO_2 > 71$ wt.% are zircon-saturated melts (Boehnke et al., 2013). Zircon saturation is demonstrated by the fact that Zr decreases with increasing SiO_2 and decreasing melt fraction (Fig. 5a, b). Zr-saturation temperatures indicate that the parental silicic magma and the HSGs formed between 750 and 800 °C (Fig. 5c, d). To maintain these low temperatures over such a wide interval of crystallization and SiO_2 requires that water contents in the silicic parent were in excess of 6 wt.% H_2O (Fig. 4c, d) (Lee et al., submitted for publication). Our findings are consistent with the more general observation that granites in continental arcs are typically cold and wet based on their low zircon saturation temperatures (Lee and Bachmann, 2014;

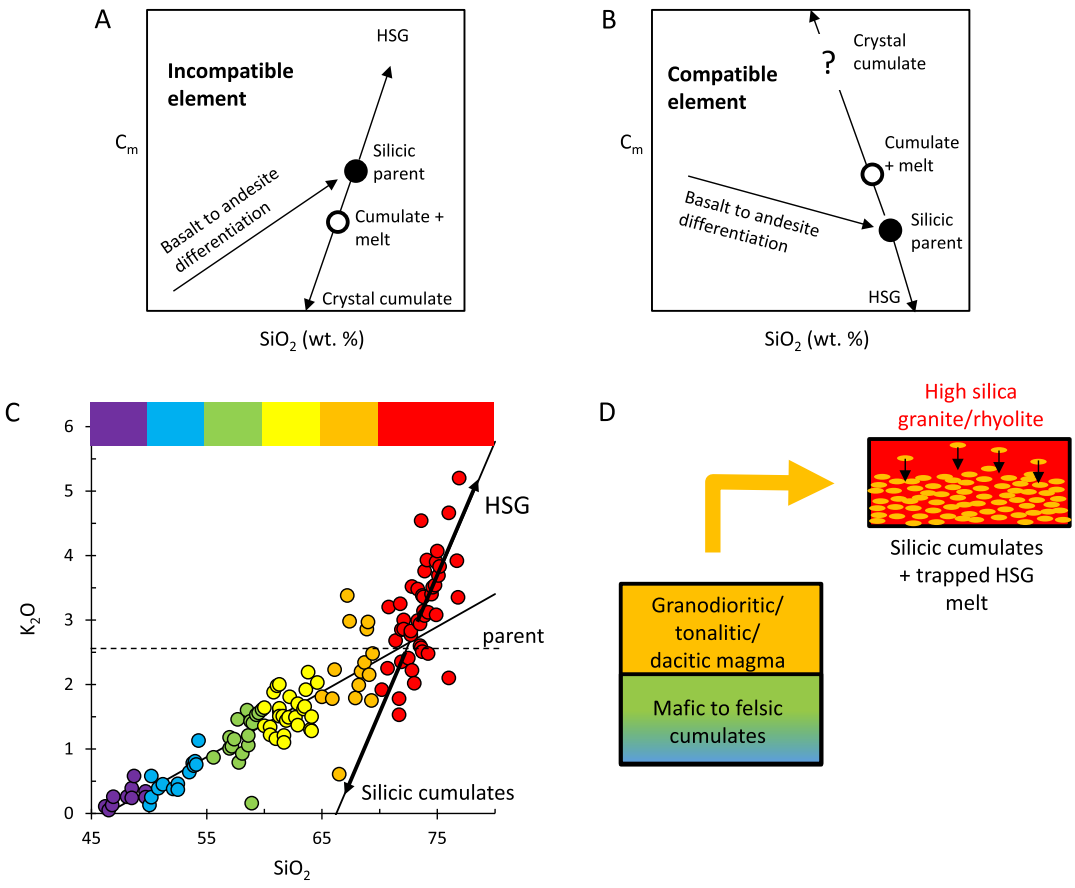

Fig. 4. A and B are schematic interpretations of elemental arrays used to determine parental silicic melt and cumulate compositions, including trapped melt content. Intersection of regression lines represents hypothetical silicic magma ("silicic parent") parental to the high silica granites (HSGs). Residual melts formed by crystallization of this silicic parent generate HSGs, which will be enriched in incompatible elements (A) but depleted in compatible elements (B). Segregation of HSG leaves behind a silicic crystal cumulate with very low incompatible element concentrations and high compatible element concentrations. SiO_2 content of the crystal cumulate is constrained with incompatible element systematics but unconstrained with compatible elements. Cumulate with trapped melt has intermediate compositions between crystal cumulate and silicic parent but must be collinear. C. K_2O versus SiO_2 color coded for SiO_2 content along with arrays showing how the elemental array method is applied to real data. D. Schematic diagram showing how parental silicic magma (orange) differentiates into high silica granite (HSG; red) and cumulates, consisting of crystal cumulates (orange) and trapped melt (red). All concentrations presented on a volatile-free basis. (For interpretation of the references to color in this figure legend, the reader is referred to the web version of this article.)

Miller et al., 2003). Our findings may not apply to high silica rhyolites from rift zones, which are hotter, shallower and drier.

We can now combine the Rb and K contents of the cumulates and the calculated F_g into Eq. (2) to estimate the mass fraction $f_{me} \sim 0.66$ of the total melt F_g extracted into the upper layer. Using Eq. (3), we obtain a trapped melt fraction in the cumulate, f_{trap}, of 0.2–0.3, corresponding to a terminal porosity of 20–30% filled with trapped HSG melt (Fig. 6).

5. Terminal porosity and origin of HSGs by crystal settling

Because the size of our study is on the scale of a batholith, our conclusion that cumulates complementary to the HSGs attain a terminal porosity of 20-30% is likely a general feature. Important implications follow. It is because of trapped melt that the cumulate composition is similar to and hence difficult to distinguish from that of the parental magma, which is already silicic. The "missing" cumulates are thus disguised among the felsic plutons themselves. The lack of cumulates with porosities lower than 20–30% suggests a lower limit to which crystals can be packed (Fig. 6). A number of studies have suggested that magmatic crystal-rich mushes compact under their own weight, causing the expulsion of interstitial melts from the compacting crystal matrix and resulting in a decrease in porosity (Bachmann and Bergantz, 2004; Brown, 1994; McKenzie, 1985). Compaction requires the crystal-bearing matrix to deform ductilely, thus the rates of compaction are limited by the effective viscosity of the crystal framework (McKenzie, 1985). Our observations suggest that compaction is too slow compared to the lifespan of silicic plutons to be an important process in expelling HSG liquids because compaction should yield some lithologies with zero porosity. The lifespans of silicic magma chambers are thought to be between 10^3 and 10^5 y (Cooper and Kent, 2014), but compaction timescales are likely much greater than this. The fact that silicic magma bodies are cold (750–800 °C) suggests that viscosities of the crystal framework may be far too high to allow for ductile deformation during the lifespan of a silicic magma body. Thus, while compaction may be an important process in segregating melts from a crystal matrix in high temperature (>1000 °C) environments, such as in the upper mantle, compaction may not be an efficient mechanism for extracting cold, silicic liquids.

Instead, the terminal 20–30% porosity, which corresponds to an upper limit of 70–80% crystallinity, broadly coincides with theoretical (0.74) and empirical (0.68–0.74) maximum packing fraction $(1-\phi)$ of unimodal particles (Donev et al., 2004) (Fig. 6). This suggests that settling, rather than compaction, may be the dominant process by which crystals and melt segregate to generate large pools of HSGs, albeit under these high crystallinities, hindered settling (Richardson and Zaki, 1954) may be a more apt description of the process. This is an important conclusion because hindered settling, even in silicic magmas, is rapid enough to generate large volumes of crystal-poor HSG on 1–10 ky timescales (Bachmann and Bergantz, 2004; Höink et al., 2008;

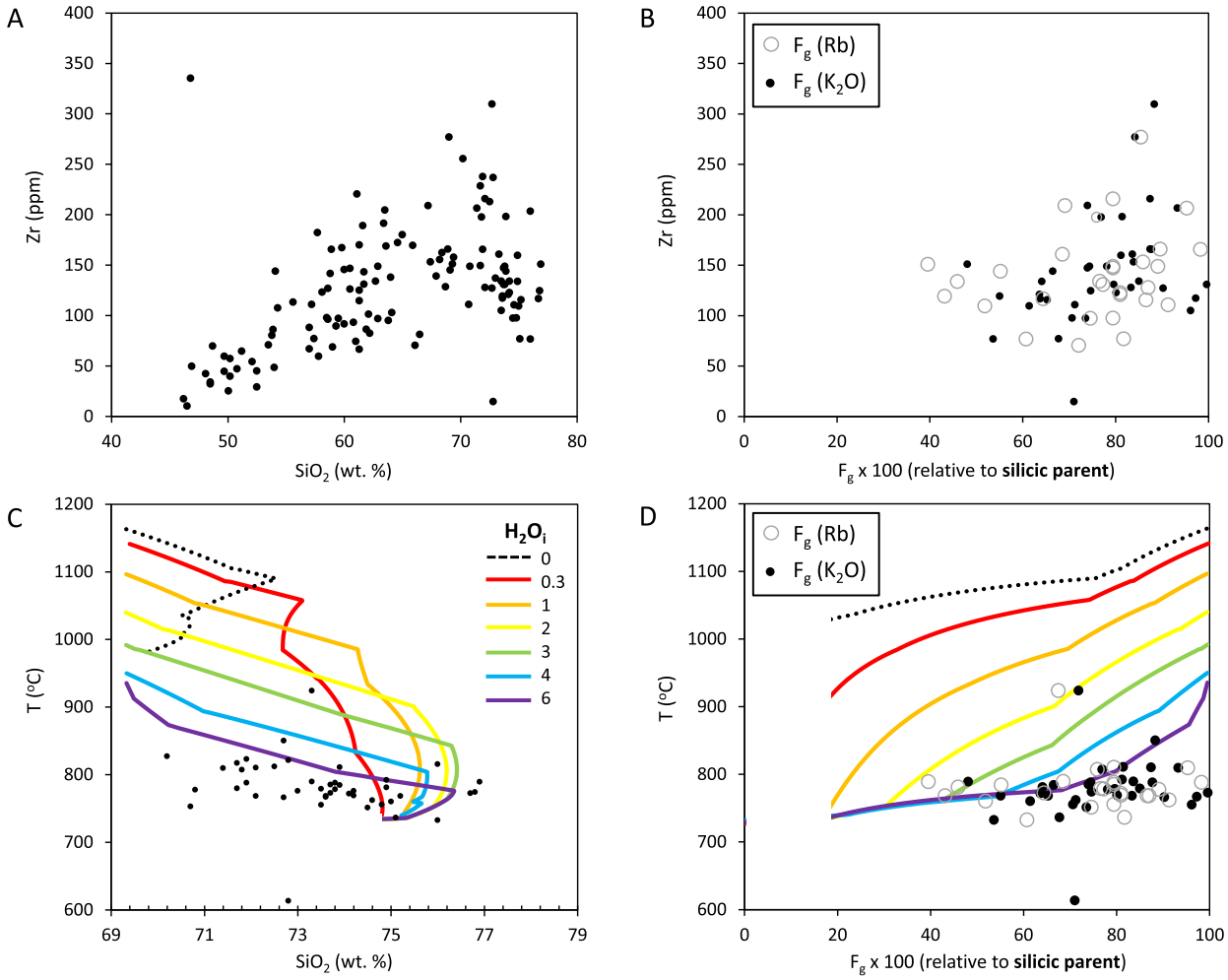

Fig. 5. A represents bulk Zr contents of western PRB plutonic rocks. Increase in Zr from 50 to 70 wt.% SiO_2 indicates a system under-saturated in zircon. Decrease in Zr with SiO_2 greater than 70 wt.% indicates saturation in zircon. B. Bulk Zr concentration for samples with $SiO_2 > 70$ wt.% (to ensure zircon saturation) versus F_g (melt fraction relative to silicic parental magma) based on Rb and K mass balance. C. Magmatic temperatures based on zircon-saturation thermometry plotted versus SiO_2 for western PRB plutons with $SiO_2 > 70$ wt.%. Also plotted are model curves relating temperature with melt SiO_2 content for different water contents, using the same models as in Fig. 4b. D. Same as in C except that *x*-axis is melt fraction F_g relative to parental silicic magma. F_g is estimated using Rb and K mass balances.

Lee et al., submitted for publication), well within the lifespans estimated for upper crustal magma chambers (Cooper and Kent, 2014).

More work is of course needed to evaluate our interpretations of the geochemical data. One direction is to evaluate whether trapped melt, as inferred from geochemical arguments, can be identified texturally. It will also be important to evaluate how crystal shape and size distributions influence the amount of trapped melt. Because plutonic rocks undergo a protracted temperature and time interval of crystallization, such textural studies will be challenging. Coupling texture with compositional mapping at micron to centimeter lengthscales is likely needed.

6. On the shallow origin of HSGs

We envision the following scenario for the generation of HSGs in continental arc environments (Fig. 7). A hydrous basalt intrudes into the lower crust or just below the crust–mantle boundary. Cooling and crystallization leads to the formation of ultramafic and mafic cumulates and residual liquids ranging from mafic to intermediate compositions (Chin et al., 2014; Jagoutz and Schmidt, 2012; Lee et al., 2006). The intermediate magma then rises into the middle or upper crust, where it continues to cool and crystallize to form highly silicic residual liquids (HSGs). The HSGs segregate from the crystals via hindered settling, generating a vertically stratified pluton composed of a crystal-poor HSG upper part and a crystal-rich cumulate mush at the bottom. Our analysis suggests that the silicic parent undergoes a maximum of 50–60% crystallization, the remaining 40–50% of the magma body being represented by HSG melt of which ~60–70% segregates to form a crystal-poor HSG layer and the remaining ~30–40% remains with the crystals, generating a cumulate mush with a terminal porosity of 20–30% filled by trapped HSG melt. Every km of HSG requires at least 2–3 km of silicic (70–71 wt.% SiO_2) melt-bearing cumulates. If the entire magmatic series from basalt to HSG indeed represents a complete liquid line of descent, the ~30-fold enrichment of incompatible trace elements in the HSGs relative to the basaltic parent implies that HSGs represent the last <5% of differentiation (Fig. 3a), which is to say, that every km of HSG requires at least 32 km of complementary crust in the form of other differentiated products, such as gabbros, diorites, granodiorites, and mafic to ultramafic cumulates. By all respects, HSGs should be volumetrically rare, <5%, in the entire crustal column).

In this context, it is interesting to examine the compositional spectrum of plutons in the PRB. The average composition of the western and eastern PRB plutons are similar, 64 ± 8.7 (1σ) and 65.6 ± 4.7 wt.% SiO_2 (Lee et al., 2007), though the eastern PRB appears to be slightly more silicic on average than the western PRB

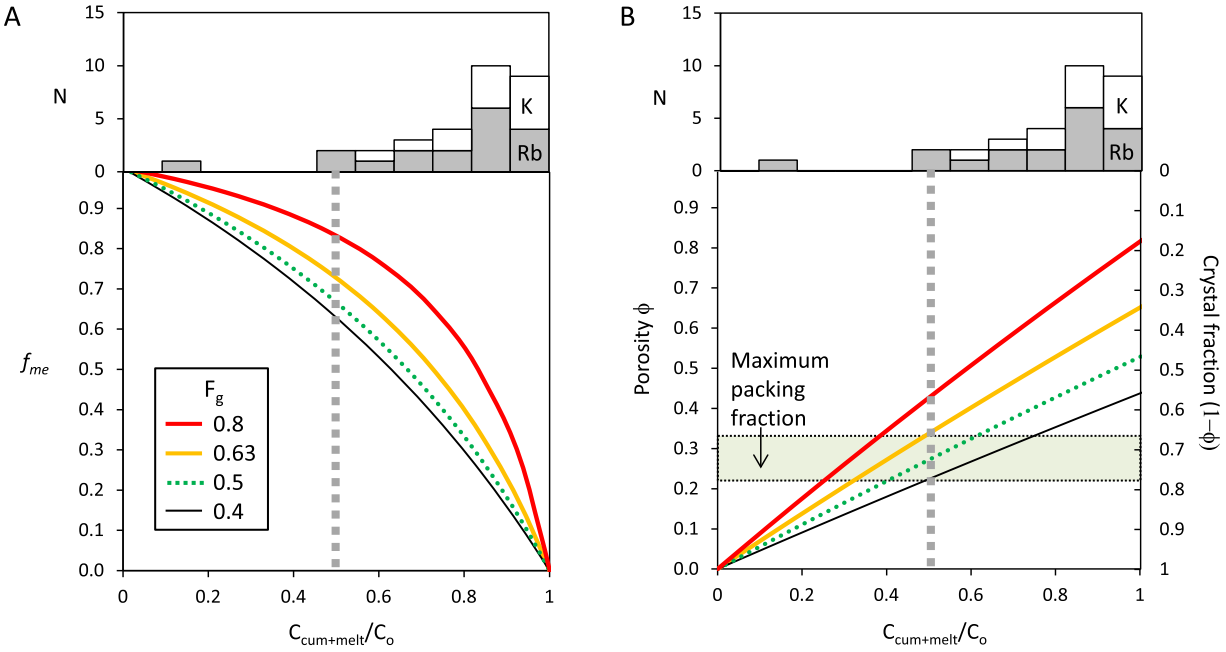

Fig. 6. A. Fraction of residual melt f_{me} that is extracted to form a layer of crystal-poor high silica granite plotted versus concentration of an incompatible element in the cumulate $C_{cum+melt}/C_o$. A value of $C_{cum+melt}/C_o$ means that the trapped melt fraction in the cumulate is zero while a value of 1 means that the cumulate is represented by 100% melt, e.g., a frozen melt. Different curves correspond to different melt fractions F in the bulk system, relative to a silicic parent. Melt fraction relative to silicic parent F_g is estimated by the inverse of the enrichment factor of an incompatible element in the melt relative to the silicic parent (as in Fig. 4b). Top panel shows observed $C_{cum+melt}/C_o$ for K and Rb. Vertical dashed line defines the lowest $C_{cum+melt}/C_o$ (extremely low value is treated as an outlier). B. Porosity and crystal fraction plotted versus $C_{cum+melt}/C_o$. Different lines correspond to different melt fractions F relative to silicic parent. Top panel as in A. Vertical dashed line as in A. Horizontal green bar defines theoretical maximum packing fraction of unimodal particles (Donev et al., 2004). (For interpretation of the references to color in this figure legend, the reader is referred to the web version of this article.)

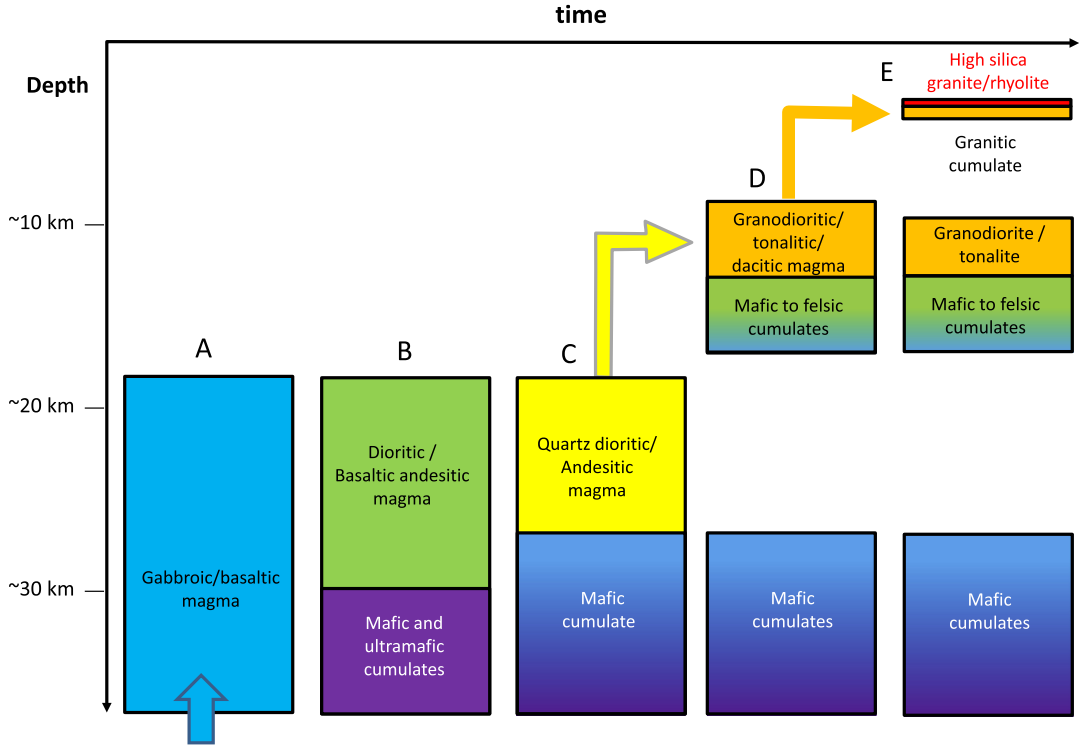

Fig. 7. Schematic cartoon (roughly to scale) illustrating the sequential formation of high silica granite (HSG). A. Basaltic magmas are intruded into the middle to lower crust. B. Basaltic magma fractionates to form mafic/ultramafic cumulates and a residual dioritic magma. C. Dioritic magmas continues to fractionate, generating mafic cumulates and residual quartz dioritic magmas. D. Quartz dioritic magmas rise into the upper crust and further differentiate, generating mafic to felsic cumulates and a granodioritic residual melt. Earlier mafic cumulates remain in the lower crust. E. Felsic melt from D segregates into a shallow crustal magma chamber and fractionates by crystal settling, generating silicic cumulates (orange) and residual high silica granitic liquids (red). The cumulates contain trapped melt. (For interpretation of the references to color in this figure legend, the reader is referred to the web version of this article.)

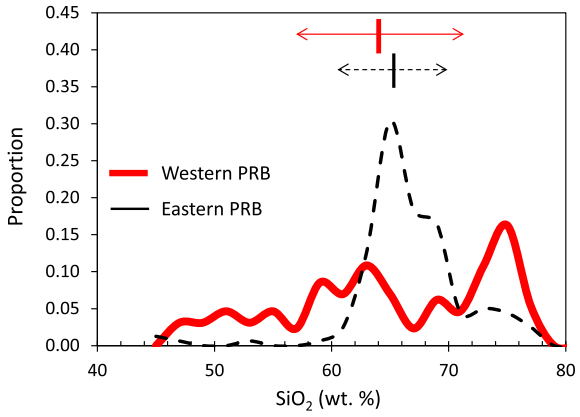

Fig. 8. SiO_2 histogram of plutonic rocks from the western (red) and eastern PRB (dashed black). Vertical bars with arrows represent average SiO_2 and standard deviation of the two PRB provinces. (For interpretation of the references to color in this figure legend, the reader is referred to the web version of this article.)

(Figs. 1 and 8). However, an important feature is that the western PRB is much more variable in composition than the eastern PRB as evidenced by the western PRBs higher standard deviation in SiO_2 (Fig. 8). Of particular interest is that HSGs make up only 16% of the eastern PRB but 37% of the western PRB *by area*, despite the fact that the eastern PRB averages more silicic than the western PRB. Equally interesting is that plutons with <60 wt.% SiO_2 make up only 3% of the eastern PRB and 30% of the western PRB. Thus, HSGs are common in batholithic provinces where mafic magmas are also common; under such conditions their areal abundance far exceeds the <5% expected from the differentiation arguments discussed above. This over-representation in the western PRB therefore implies, not surprisingly, that considerable sampling bias is introduced when the third dimension, that is, what lies beneath at depth and what has been eroded, is not sampled.

This sampling bias, nevertheless, may provide valuable insights into the conditions at which HSGs are formed. Emplacement pressures, as inferred from Al-in-hornblende barometry, in the western PRB range between 1 and 4 kbar, corresponding to depths of 4–15 km (Ague and Brimhall, 1988). Emplacement pressures in the eastern PRB range from 4 kbars to >6 kbars, corresponding to depths from 15 to >23 km. Furthermore, western PRB plutons appear to have intruded in an extensional environment and through thin crust, whereas eastern PRB plutons intruded through a compressional environment and through thicker crust (Lee et al., 2007; Morton et al., 2014). The fact that HSGs are common in the shallowly exposed western PRB but almost non-existent in the deeply exposed eastern PRB, suggests that HSGs are formed in shallow (<10 km) crustal magma chambers and not in the middle to lower crust. The association with mafic plutons provides additional support that the HSGs derive from these mafic magmas, consistent with the similar $^{87}Sr/^{86}Sr$ of mafic and felsic plutons in the western PRB (Clausen et al., 2014; Lee et al., 2007). Exactly why HSGs are dominantly of upper crustal origin is unclear.

7. Conclusions

In summary, our observations indicate that the crystal cumulates predicted to complement HSGs are among the plutons themselves, disguised to geochemically resemble frozen liquids due to the retention of 20–30% trapped HSG melt. The coincidence of trapped melt fractions with minimum packing porosity suggests that these crystal–melt aggregates form by settling instead of by compaction. Detailed micro-textural studies of plutonic rocks may provide further insight. Mass balance constraints indicate that HSGs represent <5% residual melts from fractional crystallization of mafic parents. However, we show here that HSGs are predominantly formed in shallow (<10 km) magma chambers, making them appear more common in shallowly eroded batholiths.

Acknowledgements

Discussions with Helge Gonnermann, Olivier Bachmann, Rajdeep Dasgupta, Michael Farner, Pranabendu Moitra and especially Sarah Gelman are greatly appreciated. This work was supported by NSF OCE-1338842. We thank Calvin Miller and Shanaka de Silva for insightful reviews.

References

Ague, J.J., Brimhall, G.H., 1988. Magmatic arc asymmetry and distribution of anomalous plutonic belts in the batholiths of California: effects of assimilation, crustal thickness and depth of crystallization. Geol. Soc. Am. Bull. 100, 912–927.
Bachl, C.A., Miller, C.F., Miller, J.S., Faulds, J.E., 2001. Construction of a pluton: evidence from an exposed cross-section of the Searchlight pluton, Ledorado Mountains, Nevada. Geol. Soc. Am. Bull. 113, 1213–1228.
Bachmann, O., Bergantz, G.W., 2004. On the origin of crystal-poor rhyolites: extracted from batholithic crystal mushes. J. Petrol. 45, 1565–1582.
Bachmann, O., Bergantz, G.W., 2008. Rhyolites and their source mushes across tectonic settings. J. Petrol. 49, 2277–2285.
Baird, A.K., Baird, K.W., Welday, E.E., 1979. Batholithic rocks of the northern Peninsular and Transverse Ranges, southern California: chemical composition and variation. In: Abot, P.L., Todd, V.R. (Eds.), Mesozoic Crystalline Rocks: Peninsular Range Batholith and Pegmatites, Point Sal Ophiolite. Dept. of Geological Sciences, San Diego State University, San Diego, pp. 111–132.
Boehnke, P., Watson, E.B., Trail, D., Harrison, T.M., Schmitt, A.K., 2013. Zircon saturation re-revisited. Chem. Geol. 351, 324–334.
Brown, M., 1994. The generation, segregation, ascent and emplacement of granitic magma: the migmatite-to-crustally derived granite connection in thickened orogenies. Earth-Sci. Rev. 36, 83–130.
Bucholz, C.E., Jagoutz, E., Schmidt, M.W., Sambuu, O., 2014. Phlogopite- and clinopyroxene-dominated fractional crystallization of an alkaline primitive melt: petrology and mineral chemistry of the Dariv Igneous complex, Western Mongolia. Contrib. Mineral. Petrol. 167.
Chin, E.J., Lee, C.-T.A., Barnes, J., 2014. Thickening, refertilization, and the deep lithosphere filter in continental arcs: constraints from major and trace elements and oxygen isotopes. Earth Planet. Sci. Lett. 397, 184–200.
Clausen, B.L., Morton, D.M., Kistler, R.W., Lee, C.-T.A., 2014. Low initial-Sr felsic plutons of the northwestern Peninsular Ranges batholith, southern California, and the role of mafic–felsic magma mixing in continental crust formation. Mem. Geol. Soc. Amer. 211, 317–344.
Cooper, K.M., Kent, A.J.R., 2014. Rapid remobilization of magmatic crystals kept in cold storage. Nature 506, 480–483.
Donev, A., Cisse, I., Sachs, D., Variano, E.A., Stillinger, F.H., Connelly, R., Torquato, S., Chaikin, P.M., 2004. Improving the density of jammed disordered packings using ellipsoids. Science 303, 990–993.
Ducea, M.N., Saleeby, J.B., 1998. The age and origin of a thick mafic–ultramafic keel from beneath the Sierra Nevada batholith. Contrib. Mineral. Petrol. 133, 169–185.
Gelman, S.E., Deering, C.D., Bachmann, O., Huber, C., Guiterrez, F.J., 2014. Identifying the crystal graveyard remaining after large silicic eruptions. Earth Planet. Sci. Lett. 403, 299–306.
Glazner, A.F., Johnson, B.R., 2013. Late crystallization of K-feldspar and the paradox of megacrystic granites. Contrib. Mineral. Petrol. 166, 777–799.
Greene, A.R., DeBari, S.M., Kelemen, P.B., Blusztajn, J., Clift, P.D., 2006. A detailed geochemical study of island arc crust: the Talkeetna arc section south–central Alaska. J. Petrol. 47, 1051–1093.
Gualda, G.A.R., Ghiorso, M.S., Lemons, R.V., Carley, T.L., 2012. Rhyolite-melts: a modified calibration of MELTS optimized for silica-rich, fluid-bearing magmatic systems. J. Petrol. 53, 875–890.
Hildreth, W., 1979. The Bishop Tuff: evidence for the origin of compositional zonation in silicic magma chambers. Geol. Soc. Am. Spec. Pap. 180, 43–75.
Hildreth, W., Wilson, C.J.N., 2007. Compositional zoning of the Bishop Tuff. J. Petrol. 48, 951–999.
Höink, T., Lee, C.-T.A., Hawthorne, J., Lenardic, A., 2008. Paleo-viscometry of magma bodies. Earth Planet. Sci. Lett. 267, 100–106.
Jagoutz, O., Schmidt, M.W., 2012. The formation and bulk composition of modern juvenile continental crust: the Kohistan arc. Chem. Geol. 298–299, 79–96.
Kistler, R.W., Peterman, Z.E., 1973. Variations in Sr, Rb, K, Na, and initial Sr^{87}/Sr^{86} in Mesozoic granitic rocks and intruded wall rocks in central California. Geol. Soc. Am. Bull. 84, 3489–3512.
Kistler, R.W., Wooden, J.L., Morton, D.M., 2003. Isotopes and ages in the northern Peninsular Ranges batholith, Southern California, United States. Geological Survey Open-File Report, 03-489. 45 pp.

Langmuir, C.H., 1989. Geochemical consequences of in situ crystallization. Nature 340, 199–205.
Lee, C.-T.A., 2014. Physics and chemistry of deep continental crust recycling. In: Treatise of Geochemistry, vol. 4, pp. 423–456.
Lee, C.-T.A., Bachmann, O., 2014. How important is the role of crystal fractionation in making intermediate magmas? Insights from Zr and P systematics. Earth Planet. Sci. Lett. 393, 266–274.
Lee, C.-T.A., Cheng, X., Horodyskyj, U., 2006. The development and refinement of continental arcs by primary basaltic magmatism, garnet pyroxenite accumulation, basaltic recharge and delamination: insights from the Sierra Nevada, California. Contrib. Mineral. Petrol. 151, 222–242.
Lee, C.-T.A., Morton, D.M., Farner, M.J., Moitra, P., submitted for publication. Making granites: outcrop evidence and model constraints for the role of water and hindered settling/compaction in segregating silicic liquids from crystal-rich magmas. Am. Mineral.
Lee, C.-T.A., Morton, D.M., Kistler, R.W., Baird, A.K., 2007. Petrology and tectonics of Phanerozoic continent formation: from island arcs to accretion and continental arc magmatism. Earth Planet. Sci. Lett. 263, 370–387.
McKenzie, D.P., 1985. The extraction of magma from the crust and mantle. Earth Planet. Sci. Lett. 74, 81–91.
Miller, C.F., McDowell, S.M., Mapes, R.W., 2003. Hot and cold granites? Implications of zircon saturation temperatures and preservation of inheritance. Geology 31, 529–532.
Mills, R.D., Coleman, D.S., Frazer, R.E., Glazner, A.F., Tappa, M.J., 2012. The general lack of igneous rocks with cumulate chemical signatures: is there an elephant in the room? In: Fall Meeting. Am. Geophysical Union, abstract V43D-2893.
Morton, D.M., Miller, F.K., Kistler, R.W., Premo, W.R., Lee, C.-T.A., Langenheim, V.E., Wooden, J.L., Snee, L.W., Clausen, B.L., Cossette, P., 2014. Framework and petrogenesis of the northern Peninsular Ranges batholith, southern California. Mem. Geol. Soc. Amer. 211, 61–143.
Putirka, K.D., Canchola, J., Rash, J., Smith, O., Torrez, G., Paterson, S.R., Ducea, M.N., 2014. Pluton assembly and the genesis of granitic magmas: insights from the GIC pluton in cross section, Sierra Nevada Batholith, California. Am. Mineral. 99, 1284–1303.
Richardson, J.F., Zaki, W.N., 1954. The sedimentation of a suspension of uniform spheres under conditions of viscous flow. Chem. Eng. Sci. 3, 65–73.